Geophysical Research Letters

Competition Between Atmospheric and Surface Parameterizations for the Control of Air-Sea Latent Heat Fluxes in Two Single-Column Models

Olivier Torres[1] [ID], Pascale Braconnot[1], Frédéric Hourdin[2] [ID], Romain Roehrig[3] [ID], Olivier Marti[1], Sophie Belamari[3], and Marie-Pierre Lefebvre[3,2]

[1]Laboratoire des Sciences du Climat et de l'Environnement, LSCE/IPSL, CEA-CNRS-UVSQ, Université Paris-Saclay, Gif-sur-Yvette, France, [2]Laboratoire de Météorologie Dynamique, IPSL/UPMC, Université Paris 06/Sorbonne Université/CNRS, Paris, France, [3]CNRM, Université de Toulouse, Météo-France, CNRS, Toulouse, France

Abstract A single-column model approach conducted in the context of the Madden–Julian Oscillation through the CINDY2011/Dynamics of the Madden–Julian Oscillation field campaign is used to disentangle the respective role of the parameterizations of surface turbulent fluxes and of model atmospheric physics in controlling the surface latent heat flux. The major differences between the models used in this study occur during the suppressed phases of deep convection. They are attributed to differences in model atmospheric physics which is shown to control the near-surface relative humidity and thereby the surface latent heat flux. In contrast, during active phases of deep convection, turbulent air-sea flux parameterizations impact the latent heat flux through the drag coefficient and can represent two thirds of the divergence caused by the different atmospheric physics. The combined effects need to be accounted for to improve both the representation of latent heat flux and the atmospheric variables used to compute it.

1. Introduction

Surface turbulent air-sea fluxes represent the main coupling between ocean and atmosphere circulation (Kubota et al., 2002). They are usually calculated using so-called bulk formulae (Monin & Obukhov, 1954). These empirical equations use large-scale (i.e., resolved by the model) variables to represent the air-sea exchanges that occur at a quasi-molecular scale and involve multiscale turbulent transport in the surface boundary layer (DeCosmo et al., 1996; Large & Pond, 1981). Hourdin et al. (2015) and Găinuşă-Bogdan et al. (2018) established that large-scale bias patterns in the atmospheric representation of the latent heat flux contribute to the sea surface temperature (SST) biases in the tropics, reported for decades in coupled models. Difficulties in addressing these long-standing issue probably come both from the lack of reliable observations (Găinuşă-Bogdan et al., 2015) and from the difficulty of disentangling the interplay between large-scale dynamics, atmospheric parameterizations, and surface bulk parameterization.

Despite considerable efforts, bulk formulae still have difficulties in representing air-sea fluxes especially for weak-wind stably stratified conditions (Mahrt, 2008). In general circulation models, various schemes are currently used (Beljaars 1995; Fairall et al., 2003; Large & Yeager, 2004). The associated simplifying assumptions have been shown to lead to significant differences in the computed turbulent air-sea fluxes (Brodeau et al., 2017) and in model simulations and forecasts (Seager et al., 1995). These turbulent air-sea flux parameterizations interact with the set of atmospheric parameterizations, such as those involved in turbulent diffusion, convection, or radiation. Torres et al. (2018) show that differences in drag coefficient patterns lead to differences in ocean adjustment and heat transport in coupled simulations. They also show that the results depend both on the coupling between the ocean and atmospheric boundary layer and on the way turbulent and convective processes dry and cool the low-level atmosphere.

In order to go one step further in improving our understanding of this interplay between turbulent flux parameterization and atmospheric physics at the process level, we propose an original methodology. We cross compare parameterizations of atmospheric convection and surface bulk formula in the constrained framework of a single-column model (SCM) experiment, driven by observations. Such

framework is widely used to evaluate and compare physical parameterizations without complex interaction with dynamical processes (e.g., Abdel-Lathif et al., 2018; Bechtold et al., 2000; Davies et al., 2013; Randall et al., 1996).

The experimental setup allows us to understand how the atmospheric column responds to the same surface turbulent flux parameterization implemented in the two models and to differences in parameterization in the same model. The analyses focus on the latent heat flux and are built on the hypothesis that surface evaporation is mainly controlled by the boundary layer vertical transport of humidity (Hourdin et al., 2015). We introduce in section 2 the atmospheric models and the bulk formulae implemented. Section 3 presents the CINDY2011/Dynamics of the Madden–Julian Oscillation (DYNAMO) campaign and the SCM setup used to perform the sensitivity experiments. Section 4 analyzes the impact of the different atmospheric physics on the surface latent heat flux. Section 5 discusses the role of the surface turbulent air-sea flux parameterization and the main conclusions are summarized in section 6.

2. Model and Bulk Formula Used

Two atmospheric models are considered in this study. The LMDZ atmospheric general circulation model (referred to as L hereafter) is the atmospheric component of the IPSL Coupled Model (Dufresne et al., 2013). The physical package used here is an updated version of that described in Hourdin et al. (2013). The moist convection parameterization is based on the work of Emanuel (1991), which was modified to improve the convection sensitivity to tropospheric relative humidity (Grandpeix et al., 2004). This new physical package also includes a mass flux representation of boundary layer thermals (Rio et al., 2010; Rio & Hourdin, 2008), combined with the diffusive scheme of Mellor and Yamada (1974). Cold pools fed by convective unsaturated downdraft are explicitly represented by the parameterization of Grandpeix et al. (2010). The ARPEGE-Climat atmospheric general circulation model (referred to as A hereafter) is the atmospheric component of the CNRM coupled model (Voldoire et al., 2013). The version used here (version 6.3) consists of several significant updates of the physical package (convection, microphysics, and turbulence). In particular, the new convection scheme represents in a continuous way dry, shallow, and deep convection. This new physical package was tested in the context of the CINDY2011/DYNAMO campaign in Abdel-Lathif et al. (2018).

Three surface turbulent air-sea flux parameterizations are considered in the present study: COARE 3.0 (Fairall et al., 2003) named C3 hereafter, ECUME (Belamari, 2005; Weill et al., 2003) named EC hereafter, and LMDZI used in IPSLCM5B (Dufresne et al., 2013) based on Louis (1979) and named LI hereafter. They are described in detail in Text S1 in the supporting information. Care was taken to ensure a similar implementation of the parameterization in the two models. For simulation names, first letter refer to the model (L or A) and the last two letters refer to the parameterization (LI, C3, or EC).

3 One-Dimensional Case From the CINDY2011/DYNAMO Field Campaign and SCM Setup Used for Sensitivity ExperimentsThe DYNAMO field campaign were made under the program of the cooperative Indian ocean experiment on intraseasonal variability (CINDY2011) to advance the understanding of the MJO and its representation in global models (Gottschalck et al., 2013). It provides detailed observations of the MJO (Wang et al., 2015). We consider here, the Northern Sounding array case study constructed by Ciesielski et al. (2014). From the observational records, Ciesielski et al. (2014) derive meteorological fields (wind, temperature, humidity) and various terms of the mass, energy, and water budgets (vertical velocity, horizontal advections). They are provided with a 3-hr time resolution on a 1° by 1° longitude-latitude grid with a vertical resolution of 25 hPa. We use version 3a of this data set which was not supplemented by any atmospheric model analysis data (Johnson et al., 2015; https://data.eol.ucar.edu/master_list/?project= DYNAMO).

Contrasting convective regimes are sampled over the CINDY2011/DYNAMO field campaign (Figure 1). The first and the second active periods (16 October to 3 November and 18 November to 1 December) were classified as MJO events (Achuthavarier et al., 2017; Sobel et al., 2014). In this study, we focus on the period from 4 November to 1 December. It is characterized by strong winds and horizontal moisture advections (Figure 1), and includes a suppressed MJO phase before the MJO event. During the suppressed phase, sea-surface temperatures are high, with a significant diurnal cycle (Figure 1d). This is associated with a moistening of the atmospheric column and weak atmospheric subsidence (−2 cm/s; Figure 1a). During
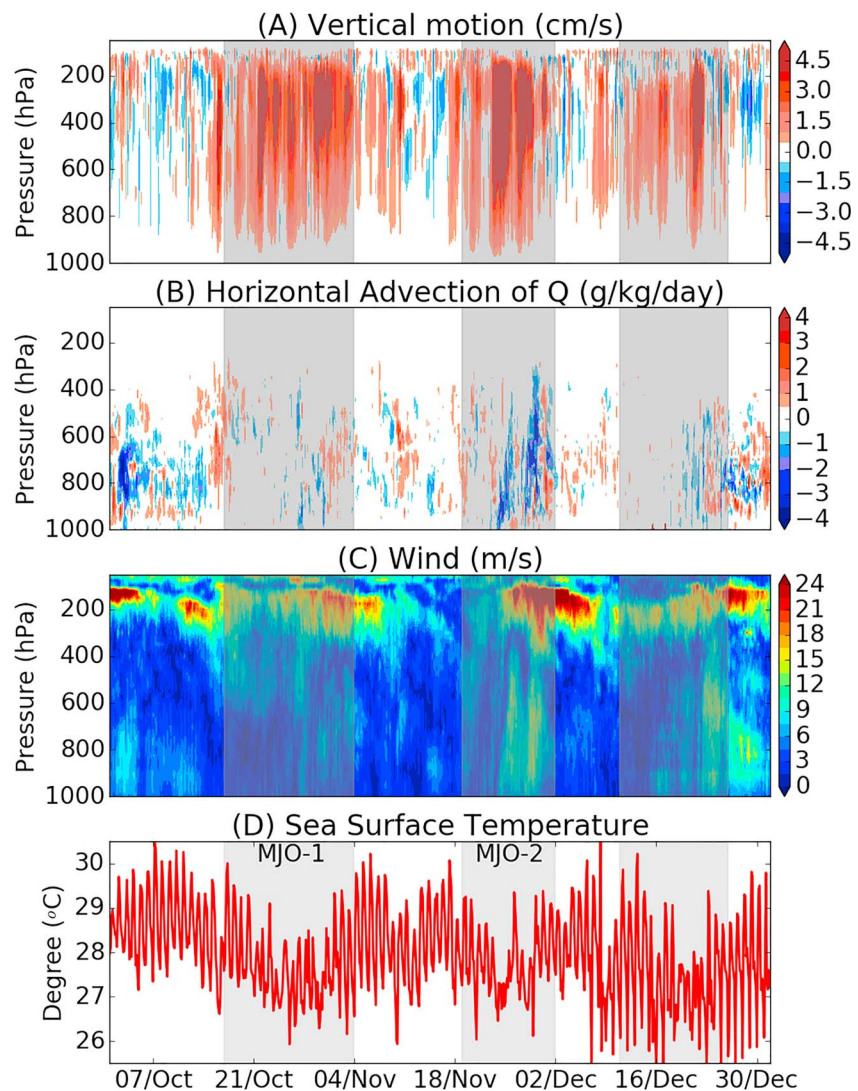
Figure 1. Imposed atmospheric and surface variables for the simulations. (a) Vertical velocity (cm/s). (b) Horizontal advection of humidity (g·kg·day). (c) Zonal wind (m/s). (d) Sea surface temperature (°C). The shading parts represent the active phases of the MJO.

the MJO active phase, SSTs are about 1 °C colder, while strong ascending motions moisten the midtroposphere (Figure 1).

The physical packages of the LMDZ and ARPEGE-Climat global models are run in the SCM framework by prescribing the large-scale horizontal advections of moisture (Figure 1b) and temperature (not shown), the large-scale vertical velocity (Figure 1a), and sea surface temperature (Figure 1d) as boundary conditions. Each SCM is run on its own vertical grid, on which observational initial profiles and forcing are linearly interpolated. The wind forcing consists in relaxing the model wind to the Northern Sounding array observed values with a 3-hr time scale for both models. Because of this experimental setup, surface fluxes and precipitation events are well synchronized in all simulations (Figures 2a2 and 2a6).

In the following, we analyze the link between the latent heat flux, flux parameterizations, atmospheric physics, and low-level temperature, humidity, and wind. For this, we rewrite the bulk formulae to introduce relative humidity in the formula (see Hourdin et al. (2015) and Text S2 in the supporting information for more details). The latent heat flux differences between two simulations (ΔLE) can be reconstructed at each time step by the sum of the following contributions:
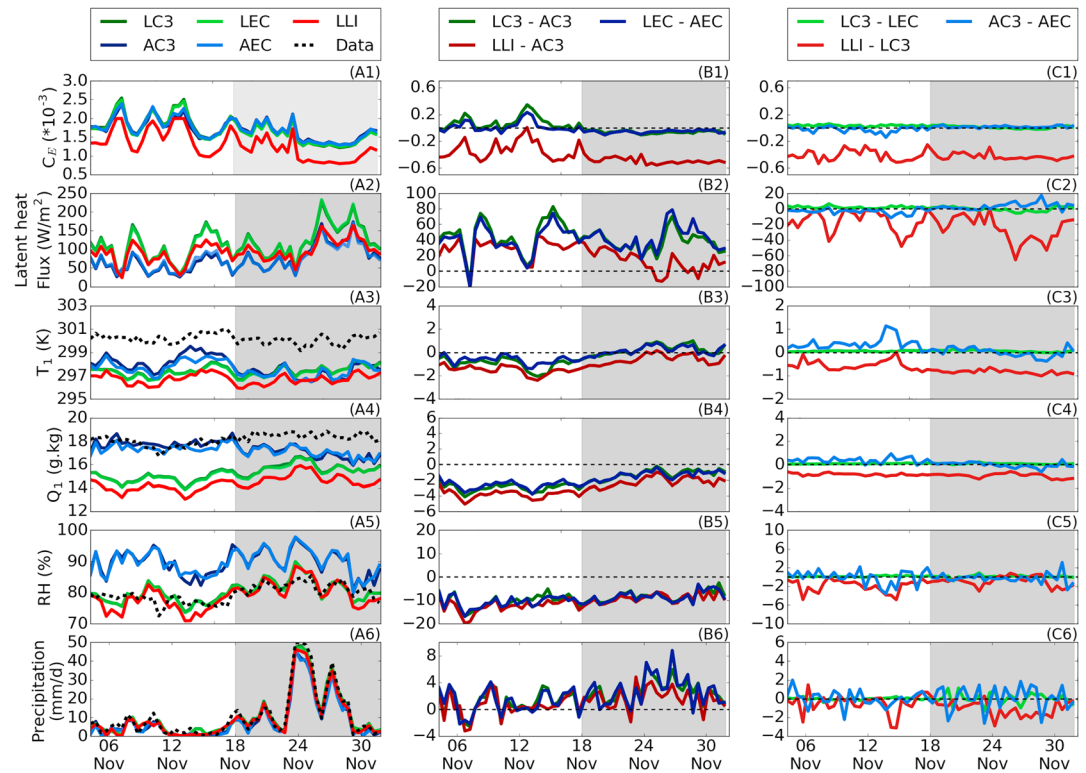
Figure 2. Daily averaged values of (1) transfer coefficient C_E, (2) latent heat flux (W/m²), (3) temperature at 1,000 hPa (K), (4) specific humidity at 1,000 hPa (g/kg), (5) relative humidity at 1,000 hPa (%), and (6) precipitation (mm/day) for (a) all the simulations, (b) differences between models, and (c) differences between parameterizations. The shading part represents the active phase of the MJO. For simulations names, first letter refers to model, L for LMDZ and A for ARPEGE-Climat, and the last two letters refer to parameterization, LI for LMDZI, C3 for Coare3.0, and EC for Ecume.

$$\Delta LE = \Delta LE_{\mathrm{dyn}} + \Delta LE_{\mathrm{sat}} + \Delta LE_{\mathrm{RH}} + \Delta LE_{\delta\mathrm{T}} + \Delta LE_{\mathrm{Ce}} \tag{1}$$

where ΔLE_{dyn}, ΔLE_{sat}, ΔLE_{RH}, $\Delta LE_{\delta\mathrm{T}}$, and ΔLE_{Ce} represent the dynamical, saturation, relative humidity, temperature, and transfer coefficient impacts on latent heat flux differences, respectively.

3. Contrasting Atmospheric Physics With Same Surface Flux Parameterization

We first characterize the impact of atmospheric physics on the representation of turbulent heat fluxes by considering the simulations run with the COARE3.0 parameterization for the two SCMs (AC3 and LC3 in Figure 2). LC3 simulates larger latent heat flux than AC3 (Figure 2b2). The average difference reaches +45.0 W/m² during the suppressed phase and +38.0 W/m² during the active phase of the MJO. This larger evaporation is obtained for a much drier atmosphere in LC3, both in terms of specific and relative humidity. This indicates that evaporation is controlled by the near-surface specific humidity rather than the opposite (a drier air would be a consequence of a weaker evaporation). The largest specific humidity differences between LC3 and AC3 (2.9 g/kg on average) are found during the suppressed phase (Figure 2b4). This contrast between the two phases is not as strong for relative humidity. The reason is that the lower atmosphere is colder during the suppressed phase (−0.96 K) and slightly warmer during the active phase (+0.22 K) in LC3 compared to AC3 (Figure 2b3). The temperature effect thus partly cancelled the effect of specific humidity. These differences in latent heat flux are always related to higher precipitation for LC3 compared to AC3 (on average +1.07 and +2.80 mm/day for the suppressed and active phases, respectively; Figure 2b6). As expected from the experimental setup, the differences in C_E between LC3 and AC3 are negligible (Figure 2).

As already mentioned, most of the latent heat flux differences between LC3 and AC3 (Figure 3a, black curve) is explained by the relative humidity term (ΔLE_{RH}, orange curve). However, differences are found between the two phases of the MJO. On average during the suppressed phase, the relative humidity (ΔLE_{RH})
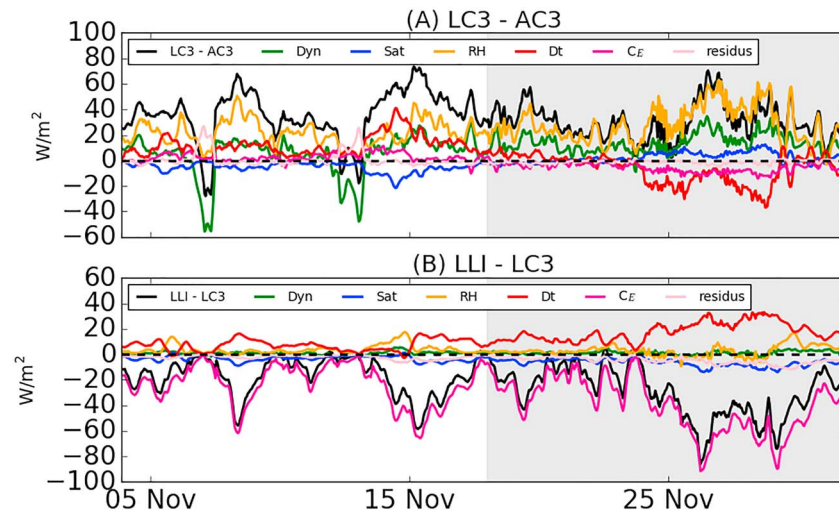
Figure 3. (a) Latent heat flux contribution differences between LC3 and AC3. (b) Latent heat flux contribution differences between LLI and LC3 (see text and Text S2 in the supporting information for the decomposition details). The shading part represents the active phase of the MJO and the residus is calculated by subtract the latent heat flux calculated by the model to the reconstructed latent heat flux.

contributes to a difference of 21.8 W/m^2 between LC3 and AC3. The second largest contribution (11.9 W/m^2) comes from the air-sea temperature contrast term ($\Delta LE_{\delta T}$, red line). The dynamical part (green line, ΔLE_{dyn}) contributes for 4.4 W/m^2 and is balanced by the impact of the saturation humidity (ΔLE_{sat}, -5.5 W/m^2). The terms ΔLE_{sat} and $\Delta LE_{\delta T}$ are additional terms in the humidity contrasts that control evaporation, which are of opposite sign by construction. During the suppressed phase, the air is somewhat colder in LC3 than in AC3, and those additional terms tend to slightly increase the contribution of relative humidity. The LMDZ atmospheric physics maintains a colder and dryer boundary layer than ARPEGE-Climat (Figure 4), which results in stronger surface latent heat flux. However, the LMDZ column-integrated water vapor is weaker (-9.9 kg/m^2). This means that although the LMDZ model has a larger latent heat flux, it stores less humidity in the atmosphere during the suppressed phases of the MJO.

On average over the suppressed phase, LC3 simulates a dryer atmospheric column below 900 hPa (-10%) and above 850 hPa with a maximum in the upper atmosphere reaching -35%. In between, LC3 simulates a slightly moister atmosphere ($+4\%$; Figure 4e). The lower troposphere is cooler (-2 K at 900 hPa), and the atmosphere above 600 hPa is warmer (Figure 4b). This is probably a footprint of a more efficient boundary layer convective vertical transport in the LMDZ resulting from the thermal plume model which explains the importance of the $\Delta LE_{\delta T}$ term in this phase. Thermals increases humidity at the top of the boundary layer, where low clouds form (around 900 hPa). The total specific humidity tendency due to turbulence, convection (shallow and deep), and large-scale advection averaged between 900 hPa and the surface (not shown) reach -0.06 and 0.005 g·kg·hr for LC3 and AC3, respectively. These differences between the two physical packages will impact SSTs in a coupled model through latent and sensible heat fluxes.

During the active convective phase, the differences between LC3 and AC3 are smaller (Figures 2 and 4). The upper atmosphere is warmer in LC3 than in AC3 (Figure 4a) suggesting a stronger convective activity, consistent with the larger convective rainfall. Concerning surface fluxes, the relative humidity (ΔLE_{RH},28.4 W/m^2) and the dynamical contributions (ΔLE_{dyn},13.8 W/m^2) account for most of the latent heat flux differences between LC3 and AC3 (Figure 3a). Here as well, the contributions of temperature contrast and saturation partly compensate. The temperature contrast contribution is much smaller than the contribution of relative humidity and changes its sign during the episode of very active convection around 26 November (Figures 3a and 4) due to a larger temperature in the LC3 simulation. This is caused by strong ascending motions that moisten and warm the first atmospheric model level more in LC3 than in AC3 (Figures 2 and 4). It decreases δT and δq and thereby the transfer coefficient which leads to a decrease of the latent heat flux. At the same time, the saturation humidity increase leads to an increase of the latent heat flux. On average, the lower troposphere is still drier in LC3 than in AC3 (-10%) but the differences in the upper
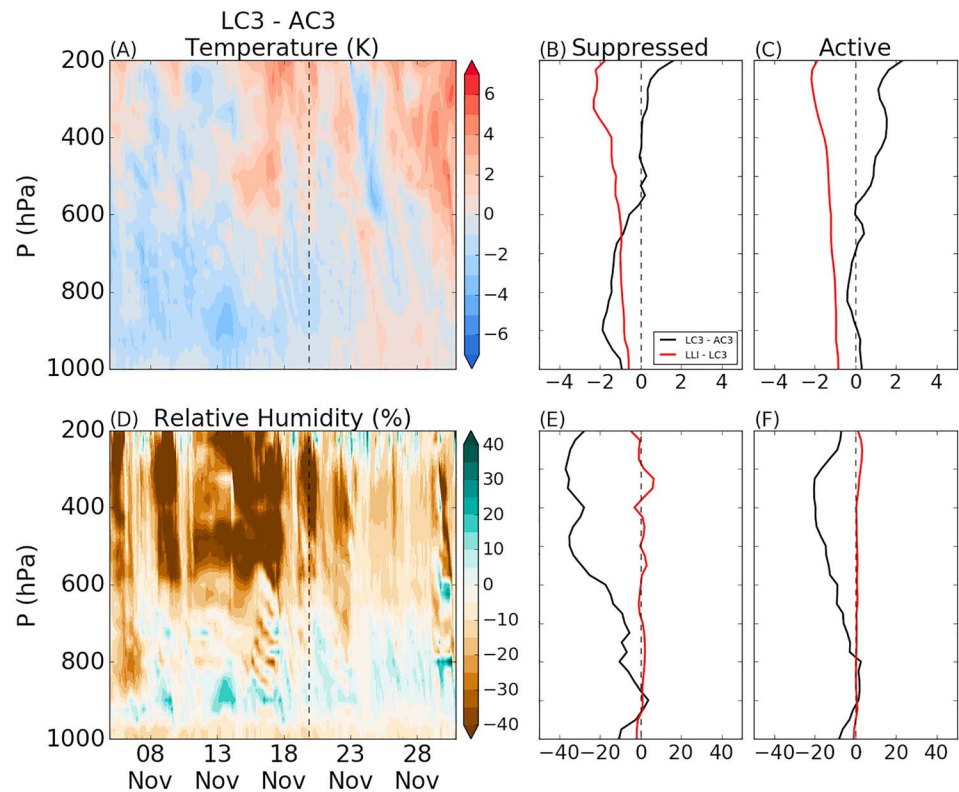
Figure 4. Differences between LC3 and AC3 simulations for the second MJO event and the suppressed phase that precedes it for (a) temperature (K) and (d) relative humidity (%). The two columns on the right represent the differences between LC3 and AC3 simulations (black) and between LLI and LC3 (red), averaged over (b and d) suppressed and (c and f) active phases of the MJO.

troposphere are reduced by a factor of 2 compared to the suppressed phase (Figures 4e and 4f). The troposphere is warmer just above the surface (+0.2 K) and above 400 hPa (+2 K), while it is slightly colder around 800 hPa (−0.4 K; Figure 4c). The LMDZ column-integrated water vapor is also smaller in active phase (−2.3 kg/m^2) but the differences between LC3 and AC3 are reduced compared to the suppressed phase. This means that the two physical packages work in a more similar way during the active convective phase.

Compared to observations, Figure 2a4 indicates that AC3 simulates closer values for specific humidity during both phases of the MJO. For both models, simulated temperatures are lower than those from the observations, regardless of the MJO phase (Figure 2a3). This systematic temperature bias was highlighted in the entire tropical band for LMDZ by Găinuşă-Bogdan et al. (2015). As shown by Abdel-Lathif et al. (2018) for ARPEGE-Climat, this dry and cold bias is also observed over the entire atmospheric column with the setup used in this study. The cold bias reaches up to −8 K near 200 hPa while the dry bias has a maximum value of −1.75 g/kg near 850 hPa. For LMDZ, the same order of magnitude is observed (not shown). In terms of near-surface relative humidity, LC3 is closer to the observations (about 80%), while AC3 overestimates it by about 10% on average during both phases of the MJO (Figure 2a5). Getting both the state variables (T, q) and relative humidity in agreement with the observations is therefore difficult.

4. Role of the Surface Flux Parameterizations

We now focus on the impact of different surface flux parameterization considering first the impact of replacing C3 by EC in the two SCMs. C3 and EC parameterizations produce very similar transfer coefficients (C_E; Figures 2a1 and 2b1). The average relative differences between them are 1.9% and −1.4% during the suppressed phase and 0.7% and 1% during the active phase, when implemented in LMDZ or ARPEGE-Climat, respectively. This results in small differences (<4 W/m^2) in the latent heat flux for the two models

(Figures 2a2 and 2c2). The results are very similar for the two models, although ARPEGE-Climat is slightly more sensitive to changes in the surface parameterization (Figures 2c1–2c6, blue line). This expected similarity was made possible thanks to a careful implementation of the parameterizations in the two models including specific details such as lower bounds put on wind speed or on transfer coefficient introduced to keep significant turbulent air-sea fluxes in weak wind regimes. To assess the impact of such implementations, two simulations were performed with the LMDZ model using LI parameterization (not shown): the first one with a threshold on wind speed at 1 m/s as in ARPEGE-Climat (it is 0.1 m/s in LMDZ) and the second one with a threshold on the transfer coefficient (0.002) as done in the LMDZ model. These thresholds induce differences in surface latent heat fluxes up to ≈ 55 W/m^2 for very weak wind conditions, much larger than changes in the formulation itself.

However, the largest impact of turbulent air-sea flux parameterization is obtained when comparing LC3 and LLI (Figure 2c1, red line). The LI parameterization always produces a lower exchange coefficient than C3 (on average −0.43 and −0.41 for the suppressed and active phases, respectively), which results in lower latent and sensible heat fluxes for both phases (Figure 2c2, red line). Using equation (1) we show that, as expected, the differences in latent heat flux between LC3 and LLI are dominated by the changes in the transfer coefficient (ΔLE_{Ce}; Figure 3b). On average, for the suppressed phase, the lower LLI C_E causes a decrease of the latent heat flux of −23.7 W/m^2. This ΔLE_{Ce} contribution is partly balanced by an increase in $\Delta LE_{\delta T}$ of +7.3 W/m^2 (Figure 3b). The other factors play a minor role in the latent heat flux differences (<5 W/m^2). The lower C_E also reduced the sensible heat flux, which cools the first model level thereby increasing the air-sea temperature difference (δT). Without any possible feedback on SST (it is prescribed), the air-sea temperature difference is directly driven by the first model level temperature.

As the decrease in the transfer coefficient is similar during the suppressed and active phases, similar mechanisms are found for the active phase. During this phase, ΔLE_{Ce} represents the major factor and drives a larger decreases latent heat flux of −40.3 W/m^2 which is compensated by a $\Delta LE_{\delta T}$ increase of +17.8 W/m^2. The net effect of this transfer coefficient (C_E) is a decrease of temperature and specific humidity at the first model level (−0.55 and −0.84 K and −0.85 and −0.95 g/kg for the suppressed and active phases, respectively; Figures 2c3 and 2c4, red line) without any change in relative humidity.

In this case, the turbulent latent heat flux differences impact the entire atmospheric column: it is drier (in terms of specific humidity) at the surface (Figures 2a4 and 2c4), and up to 2 K colder at 200 hPa (Figures 4b and 4c). The atmospheric relative humidity remains remarkably similar in the two simulations (Figures 2a5, 2c5, 4e, and 4f). Changes in the surface flux parameterization thus lead to an adjustment of the model mean atmospheric thermodynamical profiles so that relative humidity (characteristic of the atmospheric physics) remains unchanged, both in the boundary layer and in the free troposphere. In turn, relative humidity has negligible impact on the latent heat flux differences (Figure 3b).

Interestingly, replacing C3 by LI parameterization in the LMDZ model reduces the differences in latent heat flux between the LMDZ and ARPEGE-Climat SCM simulations (Figure 2b2, red line). It decreases the latent heat flux differences by 36 and 67% for suppressed and active phases, respectively, but the differences between models for low-level humidity and temperature further increase (Figures 2b3 and 2b4, red line). Similar turbulent latent heat flux is therefore obtained at the cost of an increase of the differences between the model's surface state variables (T, q). As a consequence, the original combination of atmospheric physics and surface flux parameterization of the two models minimizes the difference in terms of latent heat flux. This may reflect the fact that models were developed and tuned with a particular set of atmospheric physics and surface bulk parameterization. They therefore result from a strong effort in explicit or implicit tuning of the atmospheric physics targeting the representation of the air-sea coupling as part of the overall model climatology.

5. Conclusion

We analyzed a set of SCM simulations performed with two atmospheric general circulation models in the context of the CINDY2011/DYNAMO field campaign, which sampled several episodes of the MJO with alternating suppressed and active phase of deep convection. To understand how surface turbulent air-sea fluxes and atmospheric parameterizations, respectively, impact the surface latent heat flux, the latent heat

flux was decomposed to introduce the impact of the relative humidity near the surface. This method is particularly appropriate to assess the role of atmospheric physics and that of the bulk formula.

Compared to observations, the ARPEGE-Climat model captures well the specific humidity near the surface despite some difficulties in accurately simulating the active phase. In contrast, the LMDZ model has significant biases in both phases but captures well the near-surface relative humidity. Our analysis emphasizes that the surface turbulent latent heat flux is mostly driven by atmospheric physics during the suppressed phase of convection. Models behave more similarly during the active phase. Our analysis also indicates that, even though a model can accurately simulate the near-surface relative humidity, it might hide compensating errors that need to be further identified and understood. Indeed, each atmospheric physical package controls the near-surface relative humidity, but less clearly the model state variables (T, q). In particular, we show that near-surface relative humidity, which is most likely driven by boundary layer mixing and convective vertical transport, strongly characterizes atmospheric physics and has a strong control on the surface latent heat flux.

Although atmospheric physics has the strongest control on the surface latent heat flux during suppressed phases of deep convection, during active phases, the surface bulk parameterization can explain a large part of the latent heat flux differences and their impact should be analyzed "at constant relative humidity." In particular, the use of the LI parameterization in the LMDZ model reduces the latent heat flux differences with ARPEGE-Climat during the active phase of convection but further increases the differences in terms of state variables. Thus, changing parameterizations without considering linkages with individual processes and model physics can lead to a better representation of surface fluxes but with a potential degradation of the representation of meteorological variables.

Finally, consistent with previous studies, near-surface relative humidity is shown to be an important modeling constraint on ocean-atmosphere coupling. Our analysis further emphasizes this variable as key control on the representation of boundary layer processes (e.g., turbulence, convective transport, shallow convection), particularly during atmospheric regimes with limited deep convection. Such regimes, often considered as "simpler" because of the absence of deep convection, are especially problematic for atmospheric modeling. These regimes are highly common across the global ocean, and it is therefore necessary to work on boundary layer convection to the same extent as deep convection in atmospheric models. As such, we advocate for a better emphasis on near-surface relative humidity over the ocean, in particular a better understanding of how atmospheric processes control relative humidity and how the use of in situ observations can provide constraints on the representation of the atmospheric boundary layer over the ocean in climate models.

References

Abdel-Lathif, A. Y., Roehrig, R., Beau, I., & Douville, H. (2018). Single-column modeling of convection during the CINDY2011/DYNAMO field campaign with the CNRM Climate Model version 6. *Journal of Advances in Modeling Earth Systems.*, *10*(3), 578–602. https://doi.org/10.1002/2017MS001077

Achuthavarier, D., Wang, H., Schubert, S. D., & Sienkiewicz, M. (2017). Impact of DYNAMO observations on NASA GEOS-5 reanalyses and the representation of MJO initiation. *Journal of Geophysical Research: Atmospheres*, *122*, 179–201. https://doi.org/10.1002/2016JD025363

Bechtold, P., Redelsperger, J. L., Beau, I., Blackburn, M., Brinkop, S., Grandper, J. Y., et al. (2000). A GCSS model intercomparison for a tropical squall line observed during TOGA-COARE. II: Intercomparison of single-column models and a cloud-resolving model. *Quarterly Journal of the Royal Meteorological Society*, *126*(564), 865–888. https://doi.org/10.1002/qj.49712656405

Belamari, S. (2005). Report on uncertainty estimates of an optimal bulk formulation for surface turbulent fluxes MERSEA IP.

Beljaars, A. C. M., & Beljaars, B. A. C. M. (1995). The parametrization of surface fluxes in large-scale models under free convection. *Quarterly Journal of the Royal Meteorological Society*, *121*(522), 255–270. https://doi.org/10.1002/qj.49712152203

Brodeau, L., Barnier, B., Gulev, S. K., & Woods, C. (2017). Climatologically significant effects of some approximations in the bulk parameterizations of turbulent air–sea fluxes. *Journal of Physical Oceanography*, *47*(1), 5–28. https://doi.org/10.1175/JPO-D-16-0169.1

Ciesielski, P. E., Yu, H., Johnson, R. H., Yoneyama, K., Katsumata, M., Long, C. N., et al. (2014). Quality-controlled upper-air sounding dataset for DYNAMO/CINDY/AMIE: Development and corrections. *Journal of Atmospheric and Oceanic Technology*, *31*(4), 741–764. https://doi.org/10.1175/JTECH-D-13-00165.1

Davies, L., Jakob, C., Cheung, K., Genio, A. D., Hill, A., Hume, T., et al. (2013). A single-column model ensemble approach applied to the TWP-ICE experiment. *Journal of Geophysical Research: Atmospheres*, *118*, 6544–6563. https://doi.org/10.1002/jgrd.50450

DeCosmo, J., Katsaros, K. B., Smith, S. D., Anderson, R. J., Oost, W. A., Bumke, K., & Chadwick, H. (1996). Air-sea exchange of water vapor and sensible heat: The Humidity Exchange Over the Sea (HEXOS) results. *Journal of Geophysical Research*, *101*(C5), 12001–12016. https://doi.org/10.1029/95JC03796

Dufresne, J. L., Foujols, M. A., Denvil, S., Caubel, A., Marti, O., Aumont, O., et al. (2013). Climate change projections using the IPSL-CM5 Earth System Model: From CMIP3 to CMIP5. *Climate Dynamics*, *40*(9–10), 2123–2165. https://doi.org/10.1007/s00382-012-1636-1

Emanuel, K. A. (1991). A scheme for representing cumulus convection in large-scale models. *Journal of the Atmospheric Sciences*, *48*(21), 2313–2329. https://doi.org/10.1175/1520-0469%281991%29048%3C2313%3AASFRCC%3E2.0.CO%3B2

Fairall, C. W., Bradley, E. F., Hare, J. E., Grachev, A. A., & Edson, J. B. (2003). Bulk parameterization of air-sea fluxes: Updates and verification for the COARE algorithm. *Journal of Climate*, *16*(4), 571–591. https://doi.org/10.1175/1520-0442(2003)016<0571:BPOASF>2.0.CO;2

Găinuşă-Bogdan, A., Braconnot, P., & Servonnat, J. (2015). Using an ensemble data set of turbulent air-sea fluxes to evaluate the IPSL climate model in tropical regions. *Journal of Geophysical Research: Atmospheres*, *120*, 4483–4505. https://doi.org/10.1002/2014JD022985

Găinuşă-Bogdan, A., Hourdin, F., Traore, A. K., & Braconnot, P. (2018). Omens of coupled model biases in the CMIP5 AMIP simulations. *Climate Dynamics*, *51*(7-8), 2927–2941. https://doi.org/10.1007/s00382-017-4057-3

Gottschalck, J., Roundy, P. E., Schreck, C. J. III, Vintzileos, A., & Zhang, C. (2013). Large-scale atmospheric and oceanic conditions during the 2011–12 DYNAMO field campaign. *Monthly Weather Review*, *141*(12), 4173–4196. https://doi.org/10.1175/MWR-D-13-00022.1

Grandpeix, J.-Y., Lafore, J.-P., & Cheruy, F. (2010). A density current parameterization coupled with Emanuel's convection scheme. Part II: 1D simulations. *Journal of the Atmospheric Sciences*, *67*(4), 898–922. https://doi.org/10.1175/2009JAS3045.1

Grandpeix, J. Y., Phillips, V., & Tailleux, R. (2004). Improved mixing representation in Emanuel's convection scheme. *Quarterly Journal of the Royal Meteorological Society*, *130*(604), 3207–3222.

Hourdin, F., Găinuşă-Bogdan, A., Braconnot, P., Dufresne, J. L., Traore, A. K., & Rio, C. (2015). Air moisture control on ocean surface temperature, hidden key to the warm bias enigma. *Geophysical Research Letters*, *42*, 10,885–10,893. https://doi.org/10.1002/2015GL066764

Hourdin, F., Grandpeix, J. Y., Rio, C., Bony, S., Jam, A., Cheruy, F., et al. (2013). LMDZ5B: The atmospheric component of the IPSL climate model with revisited parameterizations for clouds and convection. *Climate Dynamics*, *40*(9–10), 2193–2222. https://doi.org/10.1007/s00382-012-1343-y

Johnson, R. H., Ciesielski, P. E., Ruppert, J. H. Jr., & Katsumata, M. (2015). Sounding-based thermodynamic budgets for DYNAMO. *Journal of the Atmospheric Sciences*, *72*(2), 598–622. https://doi.org/10.1175/JAS-D-14-0202.1

Kubota, M., Iwasaka, N., Kizu, S., Konda, M., & Kutsuwada, K. (2002). Japanese Ocean Flux data sets with use of remote sensing observations (J-OFURO). *Journal of Oceanography*, *58*(1), 213–225. https://doi.org/10.1023/A:1015845321836

Large, W. G., & Pond, S. (1981). Open ocean momentum flux measurements in moderate to strong winds. *Journal of Physical Oceanography*, *11*(3), 324–336. https://doi.org/10.1175/1520-0485(1981)011<0324:OOMFMI>2.0.CO;2

Large, W.G. & Yeager, S.G., 2004. Diurnal to decadal global forcing for ocean and sea-ice models: {The} data sets and flux climatologies. *NCAR Tech. Note*, TN-460+ST (May), p.105pp.

Louis, J. F. (1979). A parametric model of vertical eddy fluxes in the atmosphere. *Boundary-Layer Meteorology*, *17*(2), 187–202. https://doi.org/10.1007/BF00117978

Mahrt, L. (2008). Bulk formulation of surface fluxes extended to weak-wind stable conditions. *Quarterly Journal of the Royal Meteorological Society*, *134*(630), 1–10. https://doi.org/10.1002/qj.197

Mellor, G. L., & Yamada, T. (1974). A hierarchy of turbulence closure models for planetary boundary layers. *Journal of the Atmospheric Sciences*, *31*(7), 1791–1806. https://doi.org/10.1175/1520-0469(1974)031<1791:AHOTCM>2.0.CO;2

Monin, A. S., & Obukhov, A. M. (1954). Basic laws of turbulent mixing in the surface layer of the atmosphere. *Contributions of the Geophysical Institute of the Slovak Academy of Sciences*, *24*(151), 163–187.

Randall, D. A., Xu, K. M., Somerville, R. J. C., & Iacobellis, S. (1996). Single-column models and cloud ensemble models as links between observations and climate models. *Journal of Climate*, *9*(8), 1683–1697. https://doi.org/10.1175/1520-0442(1996)009<1683:SCMACE>2.0.CO;2

Rio, C., & Hourdin, F. (2008). A thermal plume model for the convective boundary layer: Representation of cumulus clouds. *Journal of the Atmospheric Sciences*, *65*(2), 407–425. https://doi.org/10.1175/2007JAS2256.1

Rio, C., Hourdin, F., Couvreux, F., & Jam, A. (2010). Resolved versus parametrized boundary-layer plumes. Part II: Continuous formulations of mixing rates for mass-flux schemes. *Boundary-Layer Meteorology*, *135*(3), 469–483. https://doi.org/10.1007/s10546-010-9478-z

Seager, R., Blumenthal, M. B., & Kushnir, Y. (1995). An advective atmospheric mixed layer model for ocean modeling purposes: Global simulation of surface heat fluxes. *Journal of Climate*, *8*(8), 1951–1964. https://doi.org/10.1175/1520-0442(1995)008<1951:AAAMLM>2.0.CO;2

Sobel, A., Wang, S., & Kim, D. (2014). Moist static energy budget of the MJO during DYNAMO. *Journal of the Atmospheric Sciences*, *71*(11), 4276–4291. https://doi.org/10.1175/JAS-D-14-0052.1

Torres, O., Braconnot, P., Marti, O., & Gential, L. (2018). Impact of air-sea drag coefficient for latent heat flux on large scale climate in coupled and atmosphere stand-alone simulations. *Climate Dynamics*, *52*(3-4), 2125–2144. https://doi.org/10.1007/s00382-018-4236-x

Voldoire, A., Sanchez-Gomez, E., Salas y Mélia, D., Decharme, B., Cassou, C., Sénési, S., et al. (2013). The CNRM-CM5.1 global climate model: Description and basic evaluation. *Climate Dynamics*, *40*(9–10), 2091–2121. https://doi.org/10.1007/s00382-011-1259-y

Wang, S., Sobel, A. H., Fridlind, A., Feng, Z., Comstock, J. M., Minnis, P., & Nordeen, M. L. (2015). Simulations of cloud-radiation interaction using large-scale forcing derived from the CINDY/DYNAMO northern sounding array. *Journal of Advances in Modeling Earth Systems*, *7*, 1472–1498. https://doi.org/10.1002/2015MS000461

Weill, A., Eymard, L., Caniaux, G., Hauser, D., Planton, S., Dupuis, H., et al. (2003). Toward a better determination of turbulent air-sea fluxes from several experiments. *Journal of Climate*, *16*(4), 600–618. https://doi.org/10.1175/1520-0442(2003)016<0600:TABDOT>2.0.CO;2

References From the Supporting Information

Bourras, D., Weill, A., Caniaux, G., Eymard, L., Bourls, B., Letourneur, S., et al. (2009). Turbulent airsea fluxes in the Gulf of Guinea during the AMMA experiment. *Journal of Geophysical Research*, *114*, C04014. https://doi.org/10.1029/2008JC004951

Charnock, H. (1955). Wind stress on a water surface. *Quarterly Journal of the Royal Meteorological Society*, *110*(C12), 639–640. https://doi.org/10.1029/2004JC002585

Fairall, C. W., Bradley, E. F., Godfrey, J. S., Wick, G. A., Edson, J. B., & Young, G. S. (1996). Coolskin and warmlayer effects on sea surface temperature. *Journal of Geophysical Research*, *101*(C1), 1295–1308. https://doi.org/10.1029/95JC03190

Fairall, C. W., Bradley, E. F., Rogers, D. P., Edson, J. B., & Young, G. S. (1996). Bulk parameterization of airsea fluxes for Tropical OceanGlobal Atmosphere CoupledOcean Atmosphere Response Experiment. *Journal of Geophysical Research*, *101*(C2), 3747–3764. https://doi.org/10.1029/95JC03205

Gouriou, Y., Andrié, C., Bourlés, B., Freudenthal, S., Arnault, S., Aman, A., et al. (2001). Deep circulation in the equatorial Atlantic Ocean. *Geophysical Research Letters*, *28*(5), 819–822. https://doi.org/10.1029/2000GL012326

Hare, JE, Persson, POG, Fairall, CW, 1999. Behavior of Charnock's relationship for high wind conditions. In pp. 252–255.

Hauser, D. (2003). The FETCH experiment: An overview. *Journal of Geophysical Research*, *108*(C3), 8053. https://doi.org/10.1029/2001JC001202

Liu, W. T., Katsaros, K. B., & Businger, J. A. (1979). Bulk parameterization of airsea exchanges of heat and water vapor including the molecular constraints at the interface. *Journal of the Atmospheric Sciences*, *36*(9), 1722–1735. https://doi.org/10.1175/15200469(1979)036<1722:BPOASE2.0.CO;2 [Accessed June 28, 2018].

Marti, O., Braconnot, P., Dufresne, J. L., Bellier, J., Benshila, R., Bony, S., et al. (2010). Key features of the IPSL ocean atmosphere model and its sensitivity to atmospheric resolution. *Climate Dynamics*, *34*(1), 1–26. https://doi.org/10.1007/s0038200906406

Mémery, L. (2005). Introduction to the POMME special section: Thermocline ventilation and biogeochemical tracer distribution in the northeast Atlantic Ocean and impact of mesoscale dynamics. *Journal of Geophysical Research*, *110*, C07S01. https://doi.org/10.1029/2005JC002976

Miller, M. J., Beljaars, A. C. M., & Palmer, T. N. (1992). The sensitivity of the ECMWI? Model to the parameterization of evaporation from the tropical oceans. *Journal of Climate*, *5*(5), 418–434. https://doi.org/10.1175/15200442(1992)005<0418:TSOTEM2.0.CO;2

Smith, S. D. (1988). Coefficients for sea surface wind stress, heat flux, and wind profiles as a function of wind speed and temperature. *Journal of Geophysical Research*, *93*(C12), 15,467–15,472. https://doi.org/10.1029/JC093iC12p15467

Webster, P. J., & Lukas, R. (1992). TOGA COARE: The Coupled Ocean–Atmosphere Response Experiment. *Bulletin of the American Meteorological Society*, *73*(9), 1377–1416. https://doi.org/10.1175/15200477(1992)073<1377:TCTCOR2.0.CO;2

Weller, R. A., Bradley, F., & Lukas, R. (2004). The interface of airsea flux component of the TOGA coupled oceanatmosphere response experiment and its impact on subsequent airsea interaction studies. *Journal of Atmospheric and Oceanic Technology*, *21*(2), 223–257. https://doi.org/10.1175/15200426(2004)021<0223:TIOAFC2.0.CO;2